INL/JOU-24-78092-Revision-0

High temperature validation of a line heat source technique for in-pile thermal conductivity determination

May 2024

Katelyn Wada, Austin D Fleming, Alyssa Bateman, Valayil Varghese, Brian Jaques, David Estrada

Changing the World's Energy Future

Idaho National Laboratory

INL/JOU-24-78092-Revision-0

High temperature validation of a line heat source technique for in-pile thermal conductivity determination

Katelyn Wada, Austin D Fleming, Alyssa Bateman, Valayil Varghese, Brian Jaques, David Estrada

May 2024

Idaho National Laboratory
Idaho Falls, Idaho 83415

http://www.inl.gov

Prepared for the
U.S. Department of Energy
Under DOE Idaho Operations Office
Contract DE-AC07-05ID14517

International Journal of Thermal Sciences 199 (2024) 108907

Contents lists available at ScienceDirect

International Journal of Thermal Sciences

journal homepage: www.elsevier.com/locate/ijts

High temperature validation of a line heat source technique for in-pile thermal conductivity determination

Katelyn Wada [a], Allyssa Bateman [a,b], Tony Valayil Varghese [a,c], Austin Fleming [d], Brian J. Jaques [a,b,d], David Estrada [a,b,d,*]

[a] Micron School of Materials Science and Engineering, Boise State University, Boise, ID, 83725, United States
[b] Center for Advanced Energy Studies, Boise State University, Boise, ID, 83725, United States
[c] Department of Electrical and Computer Engineering, Boise State University, Boise, ID, United States
[d] Idaho National Laboratory, Idaho Falls, ID, 83415, United States

ARTICLE INFO

Keywords:
Thermal conductivity
Transient line source method
High temperature
In-pile

ABSTRACT

In-pile instrumentation is critical for advancing operations and materials discovery in the nuclear industry. Ensuring optimal performance of sensors in high temperatures is the first step in demonstrating their viability in the harsh in-pile environment. This work demonstrates the high temperature capabilities of a line heat source and measurement technique previously shown to extract thermal conductivity of nuclear fuel sized samples within a laboratory environment at room temperature. This method uses a hybrid AC/DC measurement technique to obtain rapid measurements of the temperature dependent voltage change of a heater wire, which also acts as a resistance thermometer. Once the temperature profile of the heating element is extracted it is matched to a multilayered analytical model to determine the thermal conductivity of the sample. Measurements are conducted over a range of temperatures to extract the thermal conductivity as a function of temperature for 10 mm diameter 6061 aluminum samples. Each measurement had a coefficient of correlation (R^2) value higher than 0.995 when matched to its corresponding analytical model. The thermal diffusivity values for each temperature are also identified and reported. Microstructure analysis was also conducted to further characterize the material measured.

1. Introduction

Current standards for thermal properties measurements of nuclear fuel are limited to out-of-pile post irradiation examination (PIE) which introduces significant uncertainty in the behavior of fuel thermal conductivity during irradiation [1,2]. Advancements in novel in-pile technology have been highly sought after to increase the capabilities of next-generation reactors. However, high temperatures and irradiation present in-pile are difficult barriers for sensors and instrumentation [3]. In addition, thermal conductivity in particular can be difficult to extract and uniquely identify due to highly complex heat transfer equations and a large number of unknown variables [4,5].

To substantiate robustness and accuracy, techniques and sensors developed for in-pile deployment must be demonstrated in separate effects testing environments to mimic reactor conditions prior to exposing them to the combined harsh reactor conditions. In our previous work, we reported on a thermal conductivity needle probe and measurement technique [6,7] that overcame challenges of sample size limitations (i.e. the infinite medium assumption) and convective losses which limited deployment of the traditional needle probe method [2,8,9]. A minimum sample diameter of 40 mm was defined based on sensitivity parameter studies for a 4-wire probe containing thermocouple and heater wire elements [8]. A major limitation of these previous sensors that has yet to be overcome is that the electrical impedance of the insulator separating the heater and thermocouple decreases at high temperatures (1200–1800 °C) and under irradiation, allowing cross-talk between the multiple components within the probe [3,10–14]. In this work, the temperature dependent resistance of a single heater wire is used as a resistance thermometer; thus, reducing the probe's diameter, allowing for smaller diameter samples, and eliminating cross-talk between thermal elements. A DC current is applied to the heater wire to induce Joule heating while a small AC signal is superimposed to accurately measure electric resistance with a lock-in amplifier and increase signal to noise ratio. Once the measurement is

* Corresponding author. *Micron School of Materials Science and Engineering, Boise State University, Boise, ID*, 83725, *United States*.
E-mail address: daveestrada@boisestate.edu (D. Estrada).

https://doi.org/10.1016/j.ijthermalsci.2024.108907
Received 2 August 2023; Received in revised form 9 January 2024; Accepted 15 January 2024
Available online 24 January 2024

completed and the temperature profile is extracted, inverse analysis can be conducted with the use of a multilayer analytical model that encompasses the entire probe, thermal contact resistances, and sample is fitted to the measurement for thermal conductivity determination. Similar approaches to estimating parameters by solving the inverse problem are detailed in literature [15–17]. Samples as small as 10 mm in diameter were used to validate the analytical model and studies have yet to find any sample size limitations of this hybrid line source probe technique [6,7]. All measurements in the previous study were conducted at room temperature to serve as proof-of-concept of the technique. As a continuation to the room temperature results, the line heat source probe and novel measurement technique was tested at elevated temperatures to expand this technique to accurately extract thermal properties of the measured sample.

2. Materials methods

Measurements of 6061 aluminum were conducted with an MTI 4-zone tube furnace to ensure a uniform temperature distribution over the entire length of the probe (Fig. 1a). Each of the zones of the furnace were programed to start at 20 °C, heat at 3 °C per minute to 50 °C, hold for 5 min at each temperature step (up to 550 °C) and ramp at 10 °C per minute between steps (Fig. 1c). Each measurement is taken at the end of the 5-min hold to ensure the aluminum is at thermal equilibrium with the furnace. Between 2 and 4 measurements were taken at each temperature set point to ensure repeatability. The initial slow heating allows the furnace more time to successfully reach the 50 °C increment targets instead of overheating, which is less of an issue at higher temperatures. In addition, reported and utilized temperatures are that of the tube furnace thermocouple readings and not of the set temperatures. Aluminum samples, 10 mm in diameter (Fig. 1b), were measured in 50 °C increments up to 550 °C with a Type-K thermocouple (1 mm in diameter and 12 in length, which is long enough to ensure negligible end convection effects [18–20]) acting as a 2-wire probe. This sample selection allows comparison to the previous room temperature results [7] while focusing on the samples with higher thermal conductivity and minimal diameter. 6061 aluminum was chosen to show the compatibility of our technique with high thermal conductivity samples which could provide an upper limit benchmark for advanced fuels [21–23]. 6061 aluminum is also of interest for its use as metallic fuel cladding for research and test reactors [24,25].

2.1. Theory

The analytical model utilized to extract the thermal conductivity makes use of the thermal quadrupoles method [26] to model the system. Here, we use a 2-wire approach (Fig. 2b) which is simplified to an effective 1-wire geometry for modeling and calculations [7]. The effective 1-wire surrounds the heat generating elements and is depicted as a red dashed circle in Fig. 2b. The matrix representation depicting the layers of the probe, thermal contact resistance, sample, and convection is used to model the temperature of the system (equation (1)).

$$\begin{bmatrix}\theta_1\\ \varphi_1\end{bmatrix}=\begin{bmatrix}A_1 & B_1\\ C_1 & D_1\end{bmatrix}\begin{bmatrix}1 & R_{th,1}\\ 0 & 1\end{bmatrix}\begin{bmatrix}A_2 & B_2\\ C_2 & D_2\end{bmatrix}\begin{bmatrix}A_3 & B_3\\ C_3 & D_3\end{bmatrix}\begin{bmatrix}1 & R_{th,2}\\ 0 & 1\end{bmatrix}\begin{bmatrix}A_4 & B_4\\ C_4 & D_4\end{bmatrix}\begin{bmatrix}1 & 0\\ h & 1\end{bmatrix}\begin{bmatrix}\theta_3\\ \varphi_3\end{bmatrix} \quad [1]$$

Where; θ is the Laplace temperature (i.e. temperature function of the Laplace variable p), φ is the Laplace heat flux, R_{th} is thermal contact resistance, h is the convection coefficient, index 1 corresponds to the effective wire layer, index 2 is the insulator layer, 3 is the sheath layer, and 4 is the sample layer. Coefficients A, B, C, and D are represented in Table 1.

α = thermal diffusivity, p = Laplace parameter, r = radius, k = thermal conductivity, L = length, I and K = modified Bessel functions, ρ = density, c = specific heat capacity

3. Results

There are several parameters that change as temperature is increased including the thermal conductivities (k) and diffusivities (α) of the probe layers and sample. As seen in the developed sensitivity parameter studies (Fig. 3b), the thermal conductivity and diffusivity of the sample significantly overwhelm the thermal properties of the probe layers during the measurement time interval. Thus, the analytical modeling parameters of interest as temperature is increased are the samples k and α. These parameters are varied to fit the analytical model to the experimental measurements in order to achieve a thermal conductivity distribution over temperature. COMSOL Multiphysics finite element models were developed to further validate the analytical models and are depicted with the temperature plots in Fig. 3 and resulting temperature

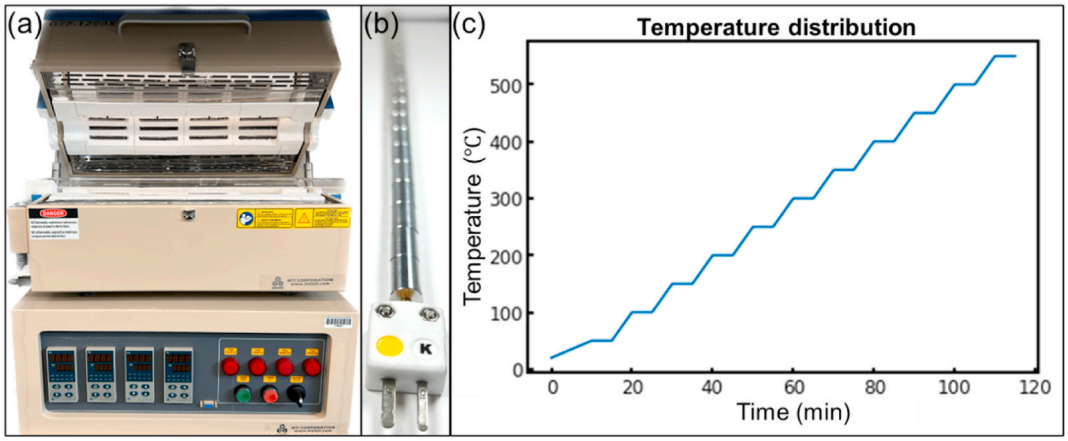

Fig. 1. (a) An image of MTI 4 zone tube furnace used to conduct high temperature measurements with the line source probe (b) an image of the Type-K thermocouple probe used in 10 mm diameter aluminum samples, and (c) a plot of the temperature vs. time programed on each temperature control unit on the furnace.

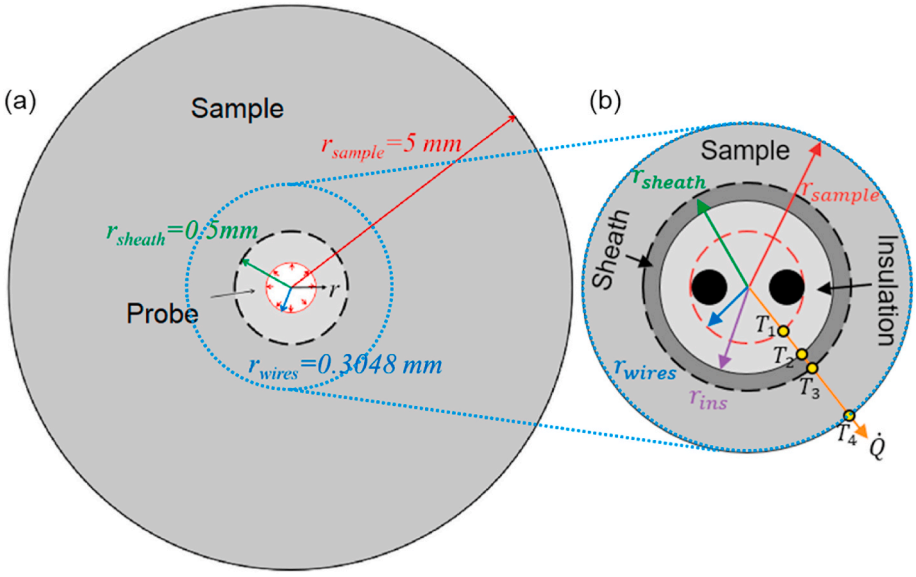

Fig. 2. (a) Cross sectional depiction of the 2-wire probe geometry and (b) effective 1-wire geometry (not to scale).

Table 1
Coefficients for the material matrices in Equation 1.

Insulation, sheath and sample layers:	Effective wire layer: average temperature solution:
$q_{1,i} = r_i\sqrt{p/\alpha_i}, q_{2,i+1} = r_{i+1}\sqrt{p/\alpha_i}$	$q_i = r_i\sqrt{p/\alpha_i}$
$A_i = q_{2,i}[I_0(q_{1,i})K_1(q_{2,i}) + I_1(q_{2,i})K_0(q_{1,i})]$	$A_i = 1$
$B_i = \frac{1}{2\pi kL}[I_0(q_{2,i})K_0(q_{1,i}) - I_0(q_{1,i})K_0(q_{2,i})$	$B_i = \frac{1}{2\pi kL}\frac{I_0(q_i)}{q_i I_1(q_i)} - \frac{1}{\rho c\pi r_i^2 Lp}$
$C_i = 2\pi kLq_{1,i}q_{2,i}[I_1(q_{2,i})K_1(q_{1,i}) - I_1(q_{1,i})K_1(q_{2,i})]$	$C_i = \rho c\pi r_i^2 Lp$
$D_i = q_{1,i}[I_0(q_{2,i})K_1(q_{1,i}) + I_1(q_{1,i})K_0(q_{2,i})$	$D_i = \frac{q_i}{2}\frac{I_0(q_i)}{I_1(q_i)}$

maps as shown in Fig. 4.

The extracted thermal conductivities and diffusivities were also plotted and shown in Fig. 5 compared to literature values. The thermal conductivity matches fairly well with differences potentially due to difference in heat treatments, microstructure, or the material itself [27–30]; however, the thermal diffusivity diverges as temperature is increased. The thermal diffusivity values for aluminum 6061 were difficult to find in literature at these temperatures so one of the distributions was calculated using the as reported density and specific heat capacities [27,29] and the others were found from a similar aluminum alloy ($AlSi_{10}Mg$ [31]). Thermal diffusivity should decrease with increasing temperature [32] which suggests some discrepancy with the literature values reported. The differences in the materials that contribute to such wide ranges in thermal conductivity and diffusivity could be better understood by also comparing microstructure. This, in turn, can provide more in-depth materials identification and usefulness in applications.

4. Discussion

4.1. Analytical model

The premise of this novel line source technique is to measure and distinguish the thermal properties of the measured sample. In addition to the k and α of the probe layers and sample, there are other parameters which change the behavior of the temperature profile. These include the thermal contact resistances between the wire and insulation ($R_{th,1}$) and between the sheath and sample layers ($R_{th,2}$) and the radii of the layers.

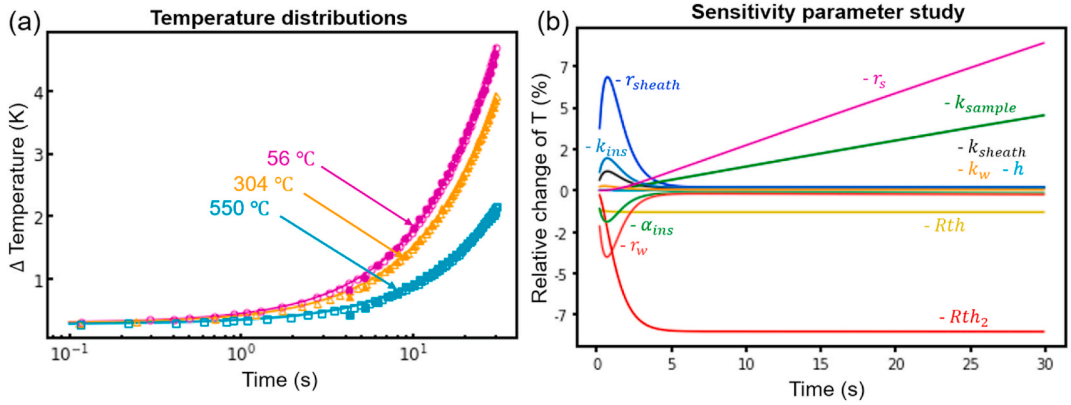

Fig. 3. (a) The resulting 56, 304, and 550 °C temperature plots including experimentally measured temperatures as solid symbols, COMSOL Multiphysics models as open symbols, and analytical models as lines. (b) Sensitivity parameter studies comparing the nominal values with a 5 % increase in the properties; sample thermal conductivity k_{sample}, sheath radius r_{sheath}, sheath thermal conductivity k_{sheath}, insulator thermal conductivity k_{ins}, wire thermal conductivity k_w, convection coefficient h, thermal contact resistance between wire and insulation Rth, thermal contact resistance between sheath and sample Rth_2, insulator diffusivity α_{ins}, and wire radius r_w.

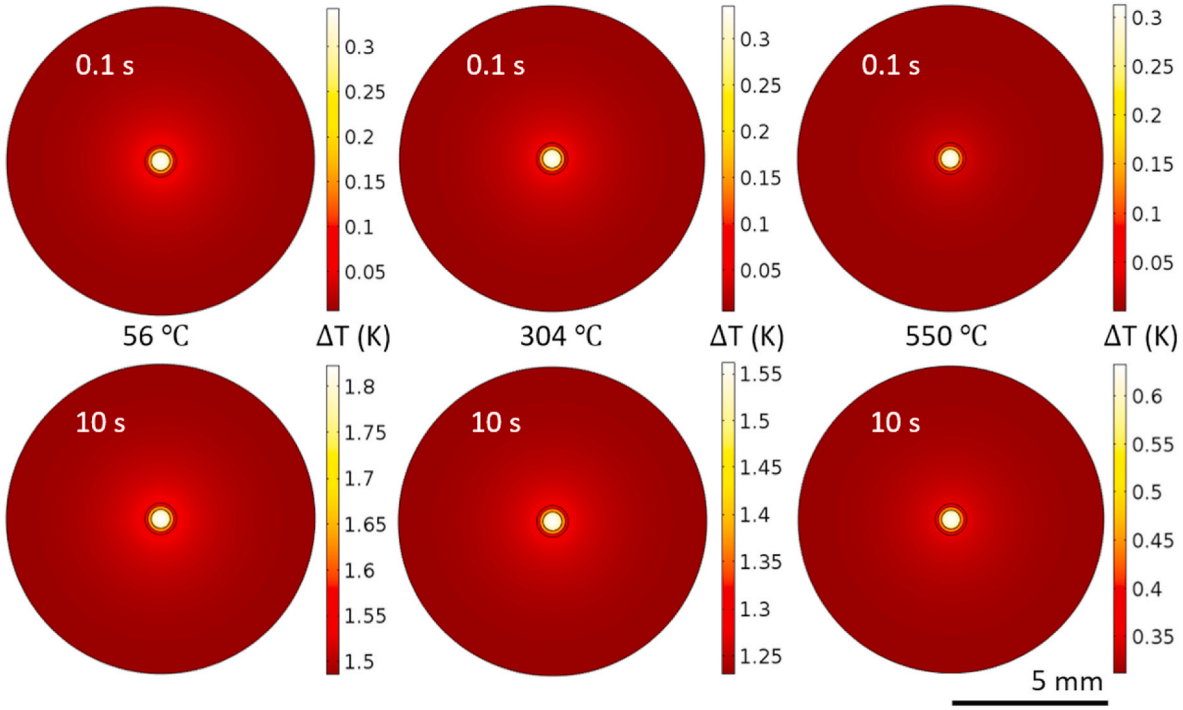

Fig. 4. COMSOL modeling results at 0.1 and 10 s for 56, 304, and 550 °C.

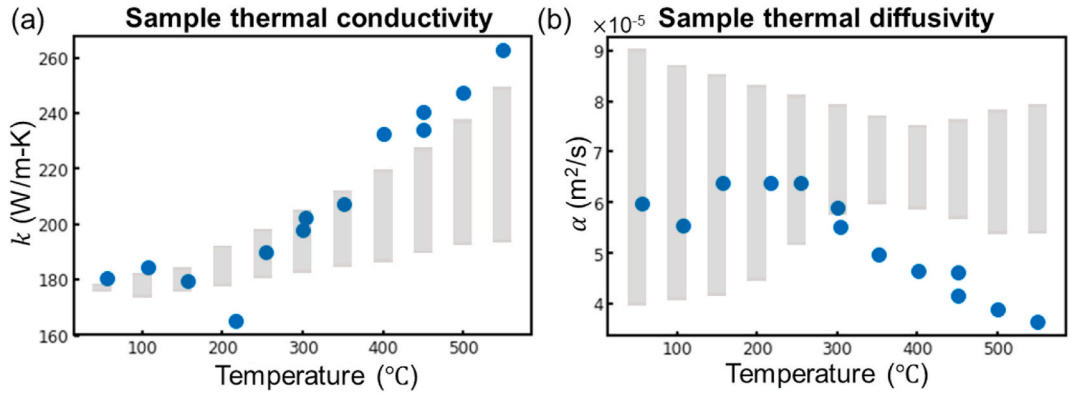

Fig. 5. The blue dots indicate the experimentally extracted values and grey bars are values from literature [27–31] **(a) The thermal conductivity, k, of the 10 mm diameter aluminum samples as a function of temperature and (b) the thermal diffusivity, α, as a function of temperature.**

After the first 5 s, $R_{th,1}$ and $R_{th,2}$ were both shown to have a constant effect on the temperature from sensitivity parameter studies. The measurements do not start until around 5 s and thus, the shape of the analytically derived temperature profile doesn't change during the measurement time interval when either thermal contact resistance parameters are changed. Changes in $R_{th,1}$ and $R_{th,2}$ would only present themselves as vertical shifts in the entire temperature profile. Thus, these parameters can be isolated from changes in k and α since they have a different effect on the temperature distribution. To simplify the fit, $R_{th,1}$ was set to 0.01 Km^2W^{-1} to be consistent with previous work [7] and $R_{th,2}$ was set to 0 to be removed from the analysis.

The radii of each of the layers also changes due to thermal expansion. However, during the measurement time interval the radius of noticeable impact is the samples. The potential change in the diameter due to thermal expansion was calculated, using thermal expansion coefficient for aluminum-6061 obtained from literature (34.2×10^6 K^{-1} at 571 °C) [27,29], and was found to be about 0.18 mm for the 10 mm diameter sample at the highest measurement temperature. This change is not large enough to overcome the sensitivity of the thermal conductivity of the sample especially at longer time scales (~30 s). At the lower temperatures measured, the thermal expansion coefficient was reported to be 24.61 $\times 10^6$ K^{-1} at 93 °C, which would produce a significantly smaller change in diameter (approximately 0.017 mm) and would have negligible effect on the (measured or analytical) temperature profile.

Furthermore, the thermal conductivity and diffusivity of the sample are not independent of each other. The values of k and α are dictated by the volumetric heat capacity ratio $k/\alpha = \rho c_P$ where ρ is the density and c_P is the heat capacity. The covariance between k and α was calculated to be −28.45 which indicates that the parameters are negatively linearly correlated. Maintaining the k/α ratio, several k and α values can be used to obtain the same fit. These parameters are varied in the analytical model to match the experimentally measured temperature distribution; however, constraints are required to obtain a viable k and α for each temperature step. The constrictions imposed were adjusted so that k and α fall within the values of a typical high thermal conductivity metals [33]. This range is further reduced when considering the room temperature values of 167 $Wm^{-1}K^{-1}$ and 6.4 $\times 10^6$ m^2s^{-1} [34]. Thermal conductivity is known to increase with temperature and thermal

diffusivity decreases with temperature [27,30,32] so these room temperature values can therefore be minimum and maximum values respectively. The ranges for the two-parameter fit are further reduced by adjusting the ranges towards higher R^2 values without changing the number of items within the ranges, which effectively increases the resolution of the fit.

4.2. Microstructure analysis

The microstructure of the aluminum samples before being heated for temperature measurements were compared against aluminum samples subject to the temperature distribution detailed in Fig. 1. Both pre-heated and post-heated aluminum samples were prepared for microscopy by grinding with SiC paper at 600, 800 and 1200 grit, followed by 3 μm diamond slurry on a Buehler TexMet C pad, then vibratory polishing in a 0.06 μm amorphous colloidal silica suspension. After polishing, samples were etched in Weck's Reagent (4 g $KMnO_4$, 1 g NaOH and 100 mL H_2O) by swirling for 120–240 s. Images were collected with an Olympus BX51 light microscope. Heat-treated samples were purposely over etched to reveal grain contrast. Grain size analysis followed ASTM standard E112: Standard Test Method for Determining Average Grain Size, specifically using the Hilliard single-circle intercept procedure with a circle circumference of 220 μ m. The procedure was repeated at four different randomly selected image locations for both as received and heat-treated samples, one of each sample is shown in Fig. 6. The average results for the grain size of the pre-heated and post-heated aluminum are 9.2 μ m with a standard deviation of 0.5 and 7.1 μ m with a standard deviation of 0.5 respectively.

An Instron 5984 was used for tensile testing of the aluminum pre- and post-heated. Dog bone structures were cut from the samples by EDM (electrical discharge machining) and inserted into custom made fixtures and secured onto a 2580-10 kN load cell. Three tensile measurements for both pre-heated and post-heated samples were conducted, one of each is depicted in Fig. 6c. The average yield strength for the pre-heated and post-heated samples was found to be 315 MPa and 81 MPa respectively.

The microstructure was investigated to further identify the measured material. A range of thermal conductivities and diffusivities for 6061 aluminum have been reported in literature, however there is a lack of corresponding microstructure analysis. Differences in microstructure could alter the thermal properties of the material leading to improper classification. The resultant grain size and yield strengths for the pre-heated and post-heated samples are consistent with literature in that temperature and yield strength have been shown to have an inversely proportional relationship [35]. Grain size has been shown to also have an inversely proportional relationship with temperature and is known to vary from 2 to 150 μ m with differences in heat treatment [36,37].

4.3. Wiedmann-franz law

The Wiedmann-Franz law was used to compare the resulting electrical conductivity (σ) calculated from the thermal conductivity (k) values acquired with the line source probe and analytical model at various temperatures with the electrical conductivity of Aluminum 6061 as reported in literature [38,39]. Utilizing the Weidemann-Franz law (equation (2)) the electrical conductivity was calculated with respect to thermal conductivity and temperature (T).

$$\frac{k}{\sigma} = LT \quad [2]$$

Here, $L = 2.44 \times 10^{-8}$ V^2K^{-2} is the Lorenz number. Using thermal conductivity and temperature values determined experimentally and plotted in Fig. 5, a range of electrical conductivity values were found to be between 1.3×10^8 and 2.0×10^7 S/m for temperatures between 50 and 550 °C. Room temperature values from literature are typically

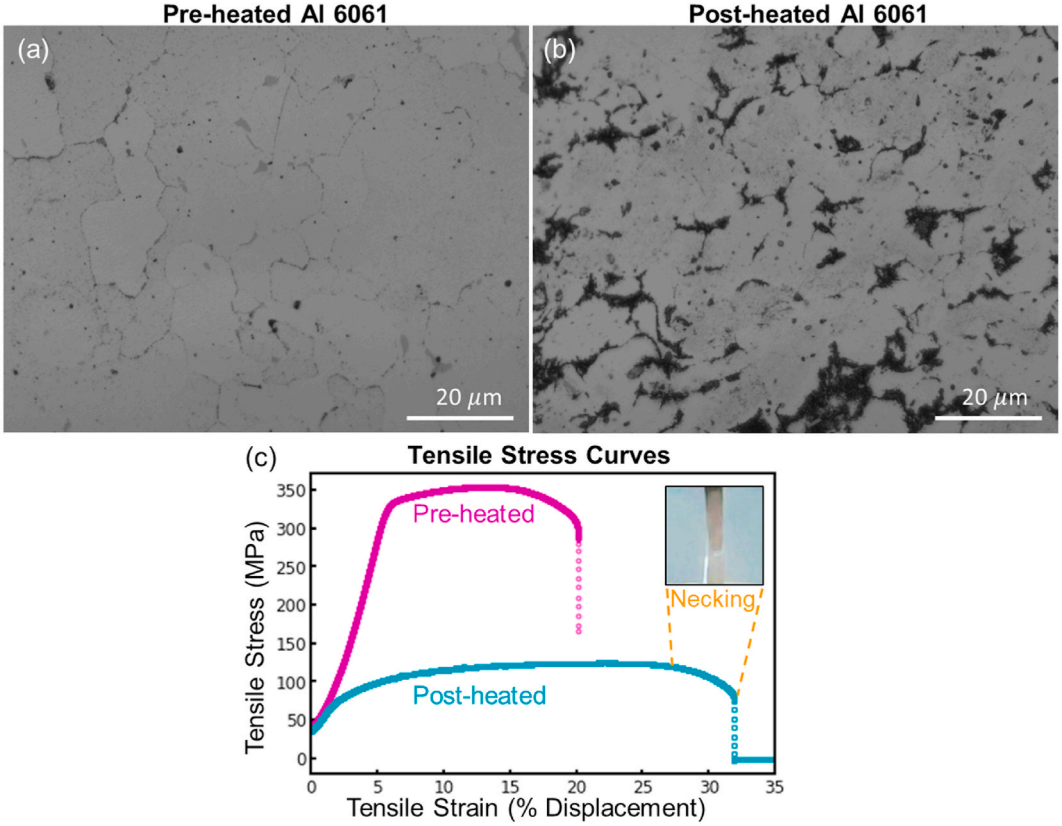

Fig. 6. Microstructure images of 6061 aluminum taken (a) before high temperature measurements and (b) after high temperature measurements. (c) Tensile stress curves of the pre-heated and post-heated 6061 aluminum.

reported in the range of 2.2×10^7 and 2.6×10^7 S/m [38,39]. Electrical conductivity is shown to decrease with increasing temperature for aluminum [40] which is consistent with the results achieved using the Weidmann-Franz law. These results further verify the thermal conductivity values obtained utilizing the line source probe.

4.4. Uncertainty analysis

According to the ISO-GUM rule [41], type B uncertainties of the experimental measurements are related to the accuracy of the SR865A 4 MHz DSP Lock-in Amplifier that measures the small AC signal, the SRS DS345 Synthesized Function Generator that provides the AC signal to be measured, and the accuracy of the measurements of the small electronics and resistance of the probe itself conducted with a Keithley DMM6500 6 ½ Digit Multimeter. This is not considering any environmental errors present; including, air drafts, humidity or noise generated from exposed electronics. To minimize the noise, the small electronics were soldered into electrical boxes. The DMM used to measure the resistances is accurate up to 0.0001 %, the function generator voltage generation is accurate up to 0.1 %, and the lock-in is accurate up to 0.01 %. Additionally, the noise in each measurement is less than 0.5 % of the measured signal. To justify the uncertainty of the measurements, the voltages measured by the lock-in were changed by 0.5 % to provide a resulting temperature distribution with maximum uncertainty from type B sources of error. This result was compared with a nominal measured temperature distribution. The error bars associated with this difference are smaller than the symbols used in Fig. 3a. In turn, this would not affect the thermal conductivity values extracted since the sensitivity of the analysis isn't sufficient to account for such small differences in the temperature distribution. In addition, the temperature coefficient of resistance of the probe was remeasured up to 550 °C. The relationship between resistance and temperature can typically be considered linear at small temperature differences however the elevated temperature of measurements conducted in this work elicits a nonlinear distribution in the resistance vs temperature curve. Comparing previous resulting temperature distributions to those recalibrated with the temperature coefficient resistance values appropriate for each temperature range resulted in a R^2 value of 0.99 and a maximum error of 3.7 % at 30 s. This small difference leads to a negligible effect on the thermal conductivity at these short time scales.

5. Conclusion

This work demonstrates the unprecedented thermal property extraction utilizing a novel line heat source probe technique at elevated temperatures for in-pile applications. Measurements were taken using 10 mm diameter aluminum samples up to 550 °C. The measurements achieved a minimum R^2 value of 0.995 when fitted to the analytical models. COMSOL Multiphysics was used to further validate the analytical modeling results. Sensitivity parameter studies were investigated to elucidate the effect of the fitting parameters which resulted in a reduction in the number of parameters necessary to extract the thermal conductivities and diffusivities at each temperature. Microstructure analysis was conducted on the materials measured to further classify the resulting thermal properties of the material measured. Future considerations should focus on bringing the measurements to other samples that can achieve even higher temperatures (1200–1800 °C) to ensure that any possible breakdown of the insulating properties of the probe has negligible effect on the measurements. In addition, irradiation testing could further validate this method as a feasible in-pile thermal conductivity measurement technique.

The authors declare that they have no known competing financial interests or personal relationships that could have appeared to influence the work reported in this paper.

CRediT authorship contribution statement

Katelyn Wada: Writing – original draft, Investigation, Formal analysis. **Allyssa Bateman:** Writing – review & editing, Methodology, Investigation. **Tony Valayil Varghese:** Writing – review & editing, Investigation, Formal analysis. **Austin Fleming:** Writing – review & editing, Project administration, Investigation, Conceptualization. **Brian J. Jaques:** Writing – review & editing, Supervision, Methodology, Investigation. **David Estrada:** Writing – review & editing, Supervision, Resources, Project administration, Methodology, Investigation, Funding acquisition, Formal analysis, Conceptualization.

Declaration of competing interest

The authors declare the following financial interests/personal relationships which may be considered as potential competing interests: David Estrada reports equipment, drugs, or supplies was provided by US Department of Energy. Katelyn Wada reports financial support was provided by US Department of Energy.

Data availability

Data will be made available on request.

Acknowledgements

This work was prepared as an account of work sponsored by the U.S. Department of Energy, Office of Nuclear Energy Advanced Sensors and Instrumentation program under DOE Contract DE- AC07-05ID14517. Neither the U.S. Government nor any agency thereof, nor any of their employees, makes any warranty, expressed or implied, or assumes any legal liability or responsibility for the accuracy, completeness, or usefulness, of any information, apparatus, product, or process disclosed, or represents that its use would not infringe privately owned rights. References herein to any specific commercial product, process, or service by trade name, trademark, manufacturer, or otherwise, does not necessarily constitute or imply its endorsement, recommendation, or favoring by the U.S. Government or any agency thereof. The views and opinions of authors expressed herein do not necessarily state or reflect those of the U.S. Government or any agency thereof. Additionally, this material is based upon work supported under a University Nuclear Leadership Program Graduate Fellowship through the Department of Energy, Office of Nuclear Energy. Further acknowledgements go to Sandeep Dhakal for providing the tensile measurement process parameters for Dr. Harold Ackler's Instron 5984, in the Materials Teaching Laboratory at Boise State University, and custom fixtures made by Philip Boysen.

References

[1] B. Fox, H. Ban, J.L. Rempe, J.E. Daw, D.L. Knudson, K.G. Condie, "In-pile thermal conductivity measurement method for nuclear fuels," *Proceedings of the 30th international thermal conductivity Conference and the 18th international thermal expansion symposium*, Therm. Conduct. 30 (2009). Thermal Expansion 18.

[2] J.E. Daw, J.L. Rempe, D.L. Knudson, Hot wire needle probe for in-reactor thermal conductivity measurement, IEEE Sensor. J. 12 (8) (2012) 2554–2560, https://doi.org/10.1109/JSEN.2012.2195307.

[3] J.L. Rempe, D.L. Knudson, J.E. Daw, K.G. Condie, S. Curtis Wilkins, New sensors for in-pile temperature detection at the advanced test reactor national scientific user facility, Nucl. Technol. 175 (3) (2009) 681–691, https://doi.org/10.13182/NT11-A12515.

[4] K. Cao, D. Lesnic, M.J. Colaco, Determination of thermal conductivity of inhomogeneous orthotropic materials from temperature measurements, Inverse Probl Sci Eng 27 (10) (Oct. 2019) 1372–1398, https://doi.org/10.1080/17415977.2018.1554654.

[5] J. Guo, X.N. Chen, Z.G. Qu, Q.L. Ren, Reverse identification method for simultaneous estimation of thermal conductivity and thermal contact conductance of multilayered composites, Int. J. Heat Mass Tran. 173 (Jul) (2021), https://doi.org/10.1016/j.ijheatmasstransfer.2021.121244.

[6] K. Wada, A. Fleming, D. Estrada, Novel thermal conductivity measurement technique utilizing a transient multilayer analytical model of a line heat source

probe for extreme environments, in: Energy Technology, 2023, https://doi.org/10.1007/978-3-031-22638-0_13. Springer, 2023.
[7] K. Wada, A. Fleming, J. Eixenberger, B.J. Jaques, D. Estrada, Transient multilayer analytical model of a line heat source probe for in-pile thermal conductivity measurements, Int. J. Therm. Sci. 188 (January) (2023), https://doi.org/10.1016/j.ijthermalsci.2023.108241, 108241.
[8] C. Hollar, A. Fleming, K. Davis, R. Budwig, C. Jensen, D. Estrada, A parametric study for in-pile use of the thermal conductivity needle probe using a transient, multilayered analytical model, Int. J. Therm. Sci. 145 (August) (2019) 106028, https://doi.org/10.1016/j.ijthermalsci.2019.106028.
[9] G. Bovesecchi, P. Coppa, S. Pistacchio, A new thermal conductivity probe for high temperature tests for the characterization of molten salts, Rev. Sci. Instrum. 89 (5) (May 2018), https://doi.org/10.1063/1.5019776.
[10] Y. Nakamura, M. Sorimachi, H. Kimura, S. Matsuyama, "Radiation resistant composition, Wire and Cable (2011) 8076408.
[11] F.A. Afzal, J.E. Giutronich, Measurement of electrical conductivity of magnesium oxide single crystal at high temperature using a solar furnace, Sol. Energy 15 (2) (1973), https://doi.org/10.1016/0038-092X(73)90122-9.
[12] P. Zirkind, E.S. Freeman, Effects of radiation on the electrical conductivity of magnesium oxide, J. Chem. Phys. 41 (1964) 906–907, https://doi.org/10.1016/0022-1902(79)80164-5.
[13] C.P. Cannon, Comparative gamma radiation and temperature effects on sio2 and mgo insulated nuclear instrument cable, Transactions on Nuclear Science 29 (1) (1982) 705–708. NS-.
[14] W. Kesternich, Radiation-induced electrical degradation: an effect of surface conductance and microcracking, J. Nucl. Mater. 253 (1–3) (1998) 167–174, https://doi.org/10.1016/S0022-3115(97)00324-3.
[15] S. Kumar, R. Akula, C. Balaji, An inverse methodology to estimate the thermal properties and heat generation of a Li-ion battery, Appl. Therm. Eng. 236 (Jan. 2024) 121752, https://doi.org/10.1016/j.applthermaleng.2023.121752.
[16] S. Kumar, C. Balaji, Prediction of orthotropic thermal conductivities using bayesian-inference from experiments under vacuum conditions, Heat Tran. Eng. 44 (14) (Aug. 2023) 1171–1192, https://doi.org/10.1080/01457632.2022.2127041.
[17] S. Kumar, P.S. Jakkareddy, C. Balaji, A novel method to detect hot spots and estimate strengths of discrete heat sources using liquid crystal thermography, Int. J. Therm. Sci. 154 (2020) 106377, https://doi.org/10.1016/j.ijthermalsci.2020.106377. Aug.
[18] N.I. Kömle, et al., In situ methods for measuring thermal properties and heat flux on planetary bodies, Planet. Space Sci. 59 (8) (2011) 639–660, https://doi.org/10.1016/j.pss.2011.03.004.
[19] R.L. Marovelli, K.F. Veith, Thermal Conductivity of Rock: Measurement by the Transient Line Source Method, 1965.
[20] D5334 – 22a, Standard Test Method for Determination of Thermal Conductivity of Soil and Rock by Thermal Needle Probe Procedure 1, ASTM International, 2022, https://doi.org/10.1520/D5334-22A.
[21] W. Zhou, W. Zhou, Enhanced thermal conductivity accident tolerant fuels for improved reactor safety – a comprehensive review, Ann. Nucl. Energy 119 (2018) 66–86, https://doi.org/10.1016/j.anucene.2018.04.040.
[22] K. McCoy, C. Mays, Enhanced thermal conductivity oxide nuclear fuels by co-sintering with BeO: II. Fuel performance and neutronics, J. Nucl. Mater. 375 (2) (2008) 157–167, https://doi.org/10.1016/j.jnucmat.2007.10.014.
[23] I. Charit, Accident tolerant nuclear fuels and cladding materials, Jom 70 (2) (2018) 173–175, https://doi.org/10.1007/s11837-017-2701-3.
[24] J.K. Conrad, et al., Radiolytic gas production from aluminum coupons (alloy 1100 and 6061) in helium environments—assessing the extended storage of aluminum clad spent nuclear fuel, Materials 15 (2022) 20, https://doi.org/10.3390/ma15207317.
[25] M.X. Milagre, et al., Galvanic coupling effects on the corrosion behavior of the 6061 aluminum alloy used in research nuclear reactors, J. Nucl. Mater. 541 (2020), https://doi.org/10.1016/j.jnucmat.2020.152440.
[26] D. Maillet, J.-C. Batsale, S. Andre', A. Degiovanni, Thermal Quadrupoles, Solving the Heat Equation through Integral Transforms, 2000, https://doi.org/10.1007/978-3-030-20524-9_4.
[27] M. Sedighi, D. Afshari, F. Nazari, Investigation of the effect of sheet thickness on residual stresses in resistance spot welding of aluminum sheets, Proc Inst Mech Eng C J Mech Eng Sci 232 (4) (2018) 621–638, https://doi.org/10.1177/0954406216685124.
[28] L. Li, H. Xia, C. Tan, N. Ma, Influence of laser power on interfacial microstructure and mechanical properties of laser welded-brazed Al/steel dissimilar butted joint, J. Manuf. Process. 32 (April) (2018) 160–174, https://doi.org/10.1016/j.jmapro.2018.02.002.
[29] H. Seli, M. Awang, A.I.M. Ismail, E. Rachman, Z.A. Ahmad, Evaluation of properties and FEM model of the friction welded mild steel-Al6061-alumina, Mater. Res. 16 (2) (2013) 453–467, https://doi.org/10.1590/S1516-14392012005000178.
[30] Z. Liu, G. Wang, J. Yi, Study on heat transfer behaviors between Al-Mg-Si alloy and die material at different contact conditions based on inverse heat conduction algorithm, J. Mater. Res. Technol. 9 (2) (2020) 1918–1928, https://doi.org/10.1016/j.jmrt.2019.12.024.
[31] P. Yang, L.A. Deibler, D.R. Bradley, D.K. Stefan, J.D. Carroll, Microstructure evolution and thermal properties of an additively manufactured, solution treatable AlSi10Mg part, J. Mater. Res. 33 (23) (2018) 4040–4052, https://doi.org/10.1557/jmr.2018.405.
[32] A. Tamilarasan, Numerical Modelling of Heat Transfer and Evaporation Characteristics of Cryogenic Liquid Propellant, 2013. January.
[33] H. Oktay, Z. Argunhan, R. Yumrutaş, Comparison of heat gain values obtained for building structures with real and constant properties, Bitlis Eren Üniversitesi Fen Bilimleri Dergisi 8 (4) (2019) 1518–1532, https://doi.org/10.17798/bitlisfen.645016.
[34] ASM Handbook Committee, Properties and selection: nonferrous alloys and special-purpose materials: properties of wrought aluminum and aluminum alloys, ASM Handbook ume 2 (1990) 62–122, https://doi.org/10.1361/asmhba000.
[35] M. Schneider, F. Werner, D. Langenkämper, C. Reinhart, G. Laplanche, Effect of temperature and texture on Hall–Petch strengthening by grain and annealing twin boundaries in the MnFeNi medium-entropy alloy, Metals 9 (no. 1) (2019), https://doi.org/10.3390/met9010084.
[36] A. Gerlich, M. Yamamoto, T.H. North, Strain rates and grain growth in Al 5754 and Al 6061 friction stir spot welds, Metall Mater Trans A Phys Metall Mater Sci 38 (6) (2007) 1291–1302, https://doi.org/10.1007/s11661-007-9155-0.
[37] J. Wang, X. Chen, L. Yang, G. Zhang, Effect of preheat & post-weld heat treatment on the microstructure and mechanical properties of 6061-T6 aluminum alloy welded sheets, Mater. Sci. Eng., A 841 (Apr) (2022), https://doi.org/10.1016/j.msea.2022.143081.
[38] Electrical Conductivity and Resistivity for Aluminum and Aluminum Alloys, Iowa State University: Center for Nondestructive Evaluation: Eddy Current Testing, January, 2024. https://www.nde-ed.org/NDETechniques/EddyCurrent/ET_Tables/standardsmethods.xhtml.
[39] Metals Handbook: properties and Selection: Nonferrous Alloys and Special-Purpose Materials," ASM International 10th Ed., vol. 2, 1990.
[40] P. Yang, et al., Analysis of peak electromagnetic torque characteristics for superconducting DC induction heaters, IEEE Access 8 (2020) 14777–14788, https://doi.org/10.1109/ACCESS.2019.2963718.
[41] ISO, Uncertainty of Measurement—Part 3: Guide to the Expression of Uncertainty in Measurement (GUM:1995), Standard No, Geneva, Switzerland, 2008. ISO-IEC 98-3:2008.